Analytic Sampling-Circuit Model

Dylan F. Williams, *Senior Member, IEEE,* and Kate A. Remley, *Member, IEEE*

***Abstract*—We develop analytic expressions for the impulse response and kickout pulses of a simple sampling circuit that incorporate the nonlinear junction capacitance of the sampling diode. We examine the effects of both the time-varying junction capacitance and conductance on the impulse response and kickout pulses, and discuss their impact on the accuracy of the nose-to-nose calibration technique.**

***Index Terms*—Analytic model, nonlinear diode capacitance, nose-to-nose calibration, sampling oscilloscope.**

I. Introduction

WE DEVELOP a small-signal model for a balanced two-diode sampling circuit and derive closed-form expressions for the circuit's impulse response and kickout pulses. The small-signal model incorporates both the sampling diode's time-varying junction capacitance and conductance. We examine separately the effects of the time-varying junction capacitance and conductance on the impulse response and kickout pulses, which we define later, and show that the nonlinear junction capacitance of the sampling diode affects the impulse response and kickout pulses in very different ways. We also examine the interaction of the external sampling circuitry with the time-varying conductance, and show that the total response of the sampler cannot be described as the convolution of two separate responses, one of the diode and one of the external circuitry. Finally, we discuss the implications of these results on the accuracy of the nose-to-nose calibration, which is based on the hypothesis that the impulse response and kickout pulses have the same shape.

[1]–[3] developed analytic expressions for the impulse response and kickout pulses of sampling circuits with purely resistive diodes and constant junction capacitance. The authors concluded that asymmetry in the small-signal diode conductance causes small differences in the kickout pulses and impulse response that cannot be corrected for by the nose-to-nose calibration.

Here, we develop a small-signal model for the sampling circuit of Fig. 1 that incorporates a time-varying diode capacitance. While this analytic model cannot account for the complicated parasitics that may be incorporated in the SPICE models described in [1] or [4]–[6], it does extend the analytic models of [1]–[3], and offers a useful intuitive understanding of the roles of nonlinear diode junction capacitance and conductance asymmetry in sampler operation. In particular, the model demonstrates that when the strobe fires, the change in the diode's junction capacitance acts as an additional source for the kickout pulses, but leaves the circuit's impulse response unchanged. The manner in which the diode's junction capacitance affects these two functions results in additional differences between the kickout pulses and impulse response that are not corrected for by the nose-to-nose calibration procedure [6].

Manuscript received July 12, 2000.

The authors are with the National Institute of Standards and Technology, Boulder, CO 80303-3328 USA (e-mail: dylan@boulder.nist.gov; remley@boulder.nist.gov).

Publisher Item Identifier S 0018-9480(01)03992-8.

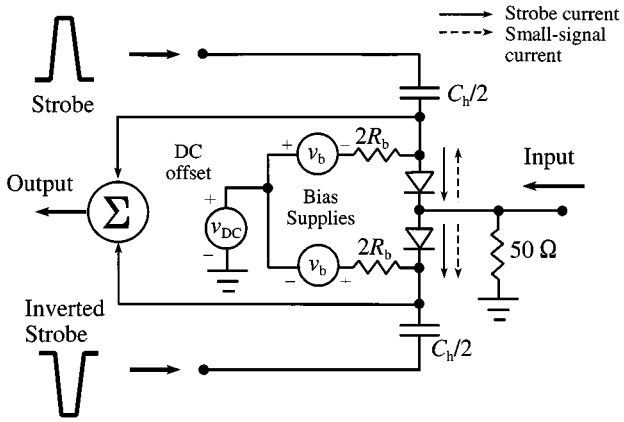

Fig. 1. Simplified schematic diagram of the two-diode sampling circuit. v_b is the diodes' reverse-bias voltage. Kickout pulses are generated when dc offset voltage v_{DC} is nonzero. The solid arrows indicate the direction of the strobe current through the diodes. The dashed arrows indicate the direction of the small-signal current due to a voltage at the input through the diodes.

II. Nose-to-Nose Calibration

Fig. 1 contains a simplified schematic diagram of a two-diode sampling circuit. The bias supplies shown in this figure place the diodes in a high-impedance reverse-biased state until the strobe fires.

Each time the strobe fires, the strobe pulse forward biases the two diodes, turning them on and lowering their impedances for a short time. Since the large-signal strobe current is in the same direction (shown by solid arrows in Fig. 1) and the circuit is balanced, the effects of the strobe current cancel at the input of the sampling circuit.

While the diodes are in their low-impedance state, a nonzero voltage at the input port of the sampling circuit causes a net charge to flow from the input port through the diodes to the hold capacitors. This small-signal current (shown by dashed arrows in Fig. 1) flows in opposite directions in the two diodes, and adds a net charge on the hold capacitors. The sampler digitizes the average voltage on the two hold capacitors after the strobe fires. This digitized voltage sample is proportional to the net charge transferred to the hold capacitor when the strobe fired, and ideally will be proportional to the voltage at the input port when the strobe fired.

In operation, a repetitive train of identical pulses is applied to the input port. The sampling circuit is used to reconstruct the

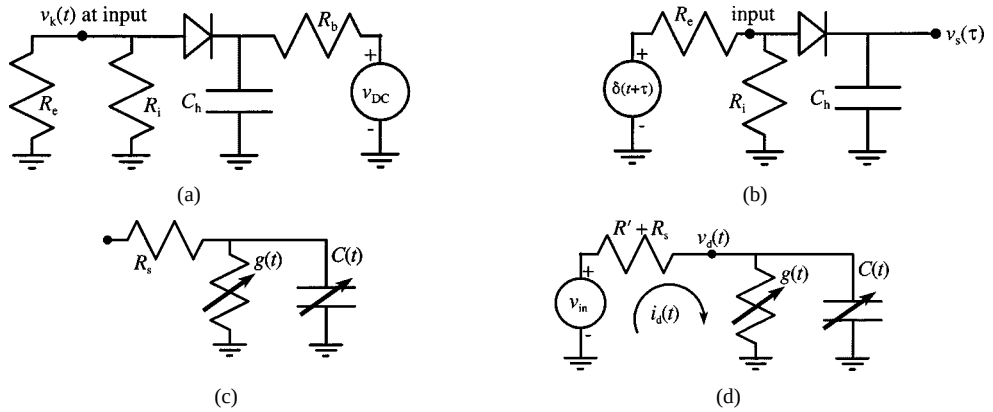

Fig. 2. Small-signal models for: (a) kickout generation, (b) sampling operation, (c) the diode, and (d) an equivalent model for both kickout generation and sampling operation. In the equivalent model, $v_{\rm in} = v_{\rm DC}$ for kickout generation and $v_{\rm in} = v_\delta(t,\tau) = [R_{\rm i}/(R_{\rm e} + R_{\rm i})]\,\delta(t+\tau)$ when determining the impulse response.

shape of an individual pulse from the input pulse train. This is accomplished by firing the strobe at a time Δt later than it fired in the previous cycle of the input pulse train. In this way, the strobe's firing time slowly "scans" across the input pulse being sampled. Since each successive digitized voltage sample corresponds to the input voltage at a time Δt later than the previous voltage sample, the shape of the pulses in the input pulse train can be reconstructed from the digitized output voltage record.

For small input signals, the output of the sampling circuit can be described as a convolution of the input signal and the "impulse response" of the sampler, which is carefully defined and explained in [4]. The first objective of this paper will be to develop an analytic expression for the impulse response of the sampling circuit shown in Fig. 1 in terms of the diode's small-signal conductance $g(t)$ and junction capacitance $C(t)$.

Rush *et al.* [7] noted that when the dc offset voltage $v_{\rm DC}$ of the sampling circuit of Fig. 1 is nonzero, it creates a train of "kickout" pulses at its input port with a shape similar to that of the circuit's impulse response. These pulses are generated by current flowing from the hold capacitors through the diodes to the input. Like the small-signal input due to voltages at the input, these currents are antiparallel. The nose-to-nose calibration [6] exploits the similarity of these kickout pulses and the circuit's impulse response to derive an estimate of the impulse response from measurements.

To perform a nose-to-nose calibration, we set the dc offset voltage of one sampling circuit to a nonzero value so that it creates a train of kickout pulses at its input port. These pulses are fed into the input port of a second sampling circuit operating in its conventional sampling mode.

When the two samplers are identical and impedance matched, and communicate through a transmission line of sufficient length, the nose-to-nose calibration reconstructs the impulse response of the circuits as the inverse Fourier transform of the square root of the Fourier transform of their nose-to-nose response. If the kickout pulses and impulse response have identical shapes, the nose-to-nose calibration accurately reconstructs the impulse response of the sampler, as demonstrated in [1]–[4].

In practice, the samplers are never identical, and the nose-to-nose calibration procedure requires three sampling oscilloscopes, additional measurements, and complex analyses to account for differences between the samplers, impedance mismatches, and imbalances in the sampling circuitry [1]–[3]. Nevertheless, the fundamental supposition of these practical three-sampler nose-to-nose calibrations is still that the kickout pulses generated by the sampling diode have the same shape as the sampler's impulse response.

III. Small-Signal Model

Fig. 2 shows the small-signal model corresponding to the sampling circuit of Fig. 1. The two balanced sampling arms, each of which contains a single sampling diode, hold capacitor, and bias circuit, have been combined, as was done in [2] and [3].

The small-signal model is based on the assumption that the capacitance $C_{\rm h}$ of the hold capacitor is large, and can be treated as a short circuit for all frequencies but dc. The resistance R' is equal to $1/(R_{\rm i}^{-1} + R_{\rm e})^{-1}$, the resistance of the parallel combination of the sampling circuit's input resistance $R_{\rm i}$ and the resistance $R_{\rm e}$ of its load, and is usually about 25 Ω. The two diodes of Fig. 1 appear in parallel in the small-signal model of Fig. 2, thus, the diode's spreading resistance $R_{\rm s}$, time-varying conductance $g(t)$, and time-varying capacitance $C(t)$ are those of the two diodes placed in parallel. That is, $R_{\rm s}$ is one-half of the spreading resistance of a single sampling diode, and $g(t)$ and $C(t)$ are twice the small-signal conductance and capacitance of the individual diodes in the circuit.

Fig. 2(a) and (b) shows small-signal models for kickout generation and sampling operation. Both the junction capacitance and conductance of the Schottky-barrier diodes used in real samplers change with applied voltage. The result is both a time-varying and generally asymmetric small-signal junction capacitance and conductance. Fig. 2(c) shows a small-signal model for the diode that includes the time-varying conductance and capacitance of the diodes.

Both the small-signal kickout circuit of Fig. 2(a) and the small-signal sampling-operation circuit of Fig. 2(b) reduce to the equivalent small-signal circuit of Fig. 2(d), with different excitation voltages $v_{\rm in}$. During both kickout generation and sampling operation, Kirchhoff's laws require that

$$v_{\rm in}(t) = (R' + R_{\rm s})i_{\rm d}(t) + v_{\rm d}(t) \tag{1}$$

where the diode's small-signal voltage and current are related by

$$\begin{aligned} i_{\rm d}(t) =& g(t)v_{\rm d}(t) + \frac{dq_{\rm j}}{dt} \\ =& g(t)v_{\rm d}(t) + \frac{d(Cv_{\rm d})}{dt} \\ =& g(t)v_{\rm d}(t) + C(t)\frac{dv_{\rm d}}{dt} + v_{\rm d}(t)\frac{dC}{dt}. \end{aligned} \tag{2}$$

Here, $q_{\rm j}$, the small-signal charge stored in the diode's junction capacitance, is equal to $Cv_{\rm d}$, the product of the junction capacitance and small-signal voltage across the diode junction. The values of g and C in (2) are determined by the large strobe signal, and can be considered to be independent of the small input signal $v_{\rm in}$. On the other hand, the small-signal voltage $v_{\rm d}$ and small-signal current $i_{\rm d}$ are the responses of the circuit to the small input signal $v_{\rm in}$, and depend on the small-signal excitation of the circuit.

Combining (1) and (2), we obtain the following differential equation in $v_{\rm d}$:

$$\begin{aligned} (R'+R_{\rm s})C(t)\frac{dv_{\rm d}}{dt} + \left[1 + (R'+R_{\rm s})\left(g(t) + \frac{dC}{dt}\right)\right] v_{\rm d}(t) \\ = v_{\rm in}(t). \end{aligned} \tag{3}$$

This is a classic linear first-order differential equation, and has the solution [8]

$$v_{\rm d}(t) = \frac{1}{u(t)}\left(u(t_0)v_{\rm d}(t_0) + \int_{s=t_0}^{t} \frac{u(s)v_{\rm in}(s)}{(R'+R_{\rm s})C(s)}ds\right) \tag{4}$$

where

$$\begin{aligned} u(t) =& \exp\left[\int_{s=t_0}^{t} \frac{1 + (R'+R_{\rm s})\big(g(s) + dC(s)\big)}{(R'+R_{\rm s})C(s)}ds\right] \\ =& \exp\left[\int_{s=t_0}^{t} \frac{a(s)}{C'(s)}ds\right] \end{aligned} \tag{5}$$

$$\begin{aligned} a(t) \equiv& 1 + (R'+R_{\rm s})\left(g(t) + \frac{dC}{dt}\right) \\ =& 1 + \left(g'(t) + \frac{dC'}{dt}\right) \end{aligned} \tag{6}$$

$g'(t) \equiv (R'+R_{\rm s})g(t)$, $C'(t) \equiv (R'+R_{\rm s})C(t)$, and t_0 is some initial time at which $v_{\rm d}$ is known.

IV. Kickout Pulses

When the sampling circuit is generating kickout pulses, the small-signal input voltage $v_{\rm in}$ is equal to the dc offset voltage $v_{\rm DC}$. The kickout voltage $v_{\rm k}(t)$ at the input port of the sampler is

$$v_{\rm k}(t) = R'i_{\rm d}(t) = \frac{R'}{R'+R_{\rm s}}\big(v_{\rm DC} - v_{\rm d}(t)\big) \tag{7}$$

where $v_{\rm d}$ is the voltage across the diode junction and $i_{\rm d}$ is the current flowing through the diode junction. To find the normalized kickout voltage $v'_{\rm k}$ defined by

$$v'_{\rm k}(t) \equiv \frac{R'+R_{\rm s}}{R'v_{\rm DC}}v_{\rm k}(t) \tag{8}$$

we substitute (4) into (7) to obtain

$$\begin{aligned} v'_{\rm k}(t) =& 1 - \frac{1}{u(t)}\left[u(t_0) + \int_{s=t_0}^{t} \frac{u(s)}{C'(s)}ds\right] \\ =& \frac{a(t)-1}{a(t)} + \frac{1}{u(t)}\int_{s=t_0}^{t} u(s)\frac{d}{dt}\left(\frac{1}{a}\right)ds \end{aligned} \tag{9}$$

where we have chosen the time t_0 to be a large negative time when $v_{\rm d} = v_{\rm DC}$. To obtain the second form in (9), we used $du/dt = au/C'$ and performed an integration by parts.

V. Impulse Response

To determine the impulse response $v_{\rm s}$ of the sampler at a time τ, we apply a Dirac delta function at the input of the sampling circuit at time $t = 0$ and fire the sampler's strobe at time $t = \tau$. We then integrate the total charge moved onto the hold capacitor during the sampling cycle to calculate the value of $v_{\rm s}(\tau)$.

This operation is equivalent to firing the sampling circuit's strobe at a fixed time and applying the Dirac delta function at the input of the sampler at time $t = -\tau$. Firing the strobe at a fixed time is more convenient to treat analytically, and we will use this approach here. When the strobe is fired at a fixed time and the delta function turns on at time $-\tau$, the small-signal input voltage $v_{\rm in}$ is equal to v_δ, where

$$v_\delta(t,\tau) = \frac{R_{\rm i}}{R_{\rm e}+R_{\rm i}}\delta(t+\tau). \tag{10}$$

Here, $-\tau$ is the time at which the impulse is applied to the sampling circuit, τ is the time at which the impulse response is determined, and δ is the Dirac delta function.

The impulse response $v_{\rm s}$ at time τ is proportional to the extra charge stored on the hold capacitors due to the small-signal input during one sampling cycle. That is, $v_{\rm s}(\tau)$ is [2], [3]

$$v_{\rm s}(\tau) = C_{\rm h}^{-1}\int_{t=-\infty}^{\infty} i_{\rm d}(t,\tau)dt \tag{11}$$

where $i_{\rm d}(t,\tau)$ is the response to the input $v_{\rm in}(t) = v_\delta(t,\tau)$ and $C_{\rm h}$ is the capacitance of the hold capacitor.

To find the normalized impulse response $v'_{\rm s}$ defined by

$$v'_{\rm s}(t) \equiv C_{\rm h}\big(R'+R_{\rm s}\big)\frac{R_{\rm e}+R_{\rm i}}{R_{\rm i}}v_{\rm s}(t) \tag{12}$$

we substitute v_δ from (10) into (4) and integrate to obtain

$$v_{\rm d}(t) = \frac{R_{\rm i}}{R_{\rm e}+R_{\rm i}}\frac{1}{u(t)}\begin{cases} 0, & t < -\tau \\ \dfrac{u(-\tau)}{C'(-\tau)}, & t > -\tau. \end{cases} \tag{13}$$

We then substitute this expression for $v_{\rm d}$ and the expression for v_δ from (10) into (1) to obtain

$$\begin{aligned} i_{\rm d}(t) =& \frac{1}{R'+R_{\rm s}}\frac{R_{\rm i}}{R_{\rm e}+R_{\rm i}} \\ & \times \left(\delta(t+\tau) - \frac{1}{u(t)}\begin{cases} 0, & t < -\tau \\ \dfrac{u(-\tau)}{C'(-\tau)}, & t > -\tau \end{cases}\right). \end{aligned} \tag{14}$$

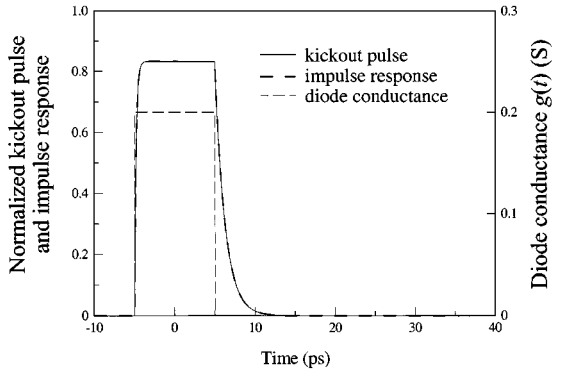

Fig. 3. The impulse response and a kickout pulse for a symmetric conductance and constant diode capacitance. In this case, the normalized impulse response and kickout pulse are identical.

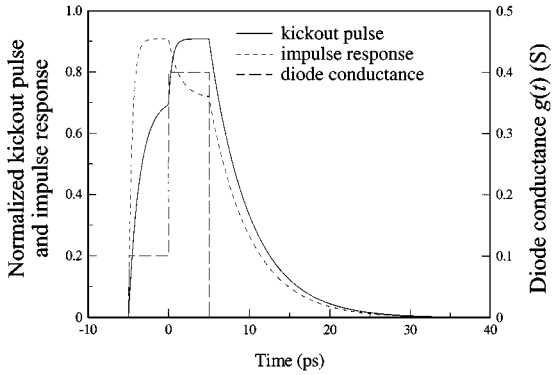

Fig. 4. A normalized kickout pulse and the impulse response for an asymmetric diode conductance and constant diode capacitance.

Performing the integral in (11), we obtain the result

$$v_{\rm s}'(\tau) = 1 - \frac{u(-\tau)}{C'(-\tau)} \int_{s=-\tau}^{\infty} \frac{ds}{u(s)} \tag{15}$$

and we have succeeded in obtaining closed-form expressions for both the impulse response of the sampling circuit and the kickout pulses it generates.

VI. Constant Capacitance

In simple cases, we can solve (9) and (15) analytically. As we shall see, this exercise is particularly insightful.

When C is constant and g is symmetric $(g(t) = g(-t))$, $v_{\rm k}'(t) = v_{\rm s}'(t)$, and the nose-to-nose calibration correctly reconstructs the impulse response [1]–[3]. Fig. 3 illustrates this, and plots $v_{\rm k}'$ and $v_{\rm s}'$ for the symmetric $g(t)$ defined by $g(t) = 0.2$ S when $|t| < t_{\rm g}/2$ and $g(t) = 0$ elsewhere. For this example, we set the capacitance $C(t) = 50$ fF, $R' + R_{\rm s} = 25\ \Omega$, and $t_{\rm g} = 10$ ps. The plot shows that, as [1]–[3] predict, the normalized kickout pulses and impulse response are equal. However, $v_{\rm k}'(t)$ is not equal to $v_{\rm s}'(-t)$. This is true only when $C = 0$.

There is an interesting observation to be made here: the kickout waveform and impulse response rise rapidly to the value $g_0'/(1 + g_0')$ (see Appendix I) when the diodes turn on at $t = -t_{\rm g}/2 = -0.5$ ps, but decay more slowly to zero when the diodes turn off again at $t = t_{\rm g}/2 = 0.5$ ps. This shows that the *RC* time constant of the circuit changes when the diode conductance changes.

Fig. 4 plots $v_{\rm k}'$ and $v_{\rm s}'$ for the asymmetric $g(t)$ defined by $g(t) = 0.1$ S in the region $-t_{\rm g}/2 < t < 0$, $g(t) = 0.4$ S in the region $0 < t < t_{\rm g}/2$, and $g(t) = 0$ elsewhere. For this example, we set $R' + R_{\rm s}$ equal to 25 Ω, and $t_{\rm g}$ equal to 10 ps and, to better illustrate the *RC* time constants, the diode junction capacitance C equal to 200 fF. This figure illustrates not only the time-reversal of the impulse response predicted by [1]–[3] and inherent in the solution for the impulse response (15), but the differences in the *RC* time constants associated with the kickout pulses and impulse response. It is evident that the leading edge of the impulse response rises much more sharply than the leading edge of the kickout pulse. As the analytic solutions tabulated in Appendix I show, this is because the rate at which the leading edge of the kickout pulse increases is set by the diode's conductance of 0.1 S during the time interval $-t_{\rm g}/2 < t < 0$, while the rate at which the leading edge of the impulse response increases is set by the diode's conductance of 0.4 S during the time interval $0 < t < t_{\rm g}/2$.

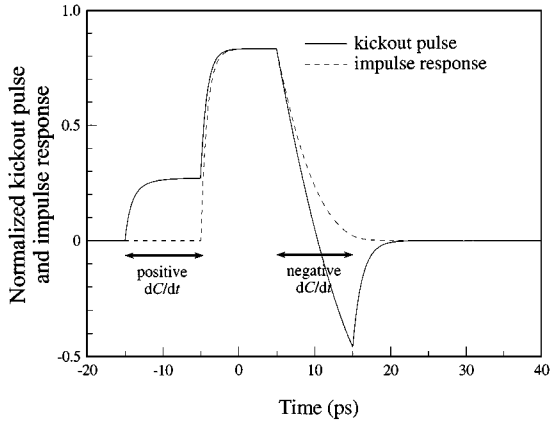

Fig. 5. A normalized kickout pulse and the impulse response for the diode conductance and capacitance plotted in Fig. 6. We set $R' + R_{\rm s}$ equal to 25 Ω.

Again, we see that the *RC* time constant associated with charging the diode's junction capacitance changes with time. We thus conclude that we cannot describe the kickout pulses or impulse response of even these simple sampling circuits as the convolution of a time-varying aperture response $g'(t)/(1+g(t))$ or $g'(-\tau)/(1+g'^{(-\tau)})$ and the time-invariant transfer function of an external *RC* circuit, as might be expected. This is because the *RC* time constant associated with charging the diode's junction capacitance is modified by the time-varying diode conductance $g(t)$ and, thus, becomes a time-varying, rather than time-invariant, quantity. These conclusions are consistent with those of [2] and [3].

VII. Time-Varying Capacitance

Fig. 5 plots the impulse response and a kickout pulse for the capacitance and conductance waveforms shown in Fig. 6. This figure illustrates the role of the time derivative dC/dt of the diode's junction capacitance C, also discussed in Fig. 6. Notice that the leading edge of the kickout pulse begins to rise as soon as dC/dt becomes positive at $t = -15$ ps.

The effect of the change in diode junction capacitance on the kickout pulse can be understood by considering the charge

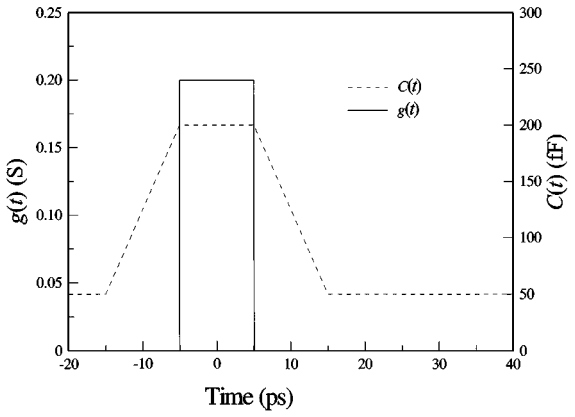

Fig. 6. Time-varying diode conductance $g(t)$ and capacitance $C(t)$ corresponding to the normalized kickout pulse and impulse response plotted in Fig. 5.

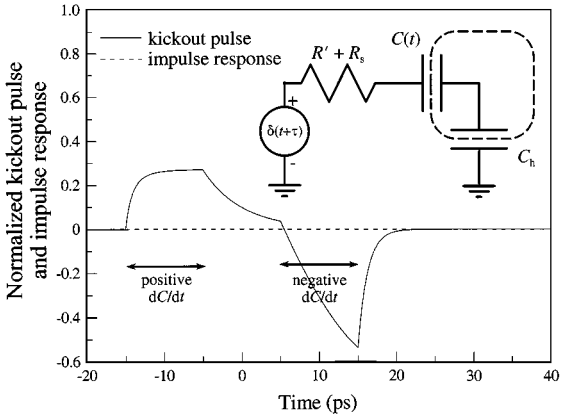

Fig. 7. Normalized kickout pulse and the impulse response for a zero diode conductance and the capacitance plotted in Fig. 6 The circuit drawn in the figure corresponds to the small-signal model for sampling operation. The total charge inside the dashed line is conserved. We set $R' + R_s$ equal to 25 Ω.

stored in the junction capacitance. When the strobe fires, the diode is forward biased, and its depletion region narrows, increasing the diode's junction capacitance. Since the sampling circuit is balanced, these large-signal strobe currents cancel at the input.

However, as the diode's junction capacitance increases suddenly, the small-signal charge $q_d = Cv_d$ stored in the junction capacitance is conserved. As a result, the small-signal voltage v_d across the junction must decrease suddenly to compensate. This sudden drop in v_d generates the early rise in the kickout pulse seen over the time region -15 ps $< t < -5$ ps in Fig. 5. Likewise, the negative overshoot of the kickout in Fig. 5 is due to the drop of diode junction capacitance back to its reversed-biased value of C_0 over the time region 5 ps $< t < 15$ ps.

Fig. 5 also shows that the changing $C(t)$ does not affect the impulse response over the time region -15 ps $< t < -5$ ps. This is because the digitized voltage on the hold capacitor at the end of the sampling cycle depends on the total charge moved onto the hold capacitor during the sampling cycle, and the net charge transferred to the hold capacitor through the diode is zero.

This can be understood with the following argument. Due to the time reversal in (15), the time region -15 ps $< t < -5$ ps of the impulse response corresponds to exciting the sampling circuit with an impulse *after* the sampling diode has turned off. Since the diode has already turned off before the excitation starts, $g(t)$ has already returned to zero, and no extra electrons flow through the diode's junction conductance due to the small-signal excitation.

Not only are electrons unable to move across the diode's junction conductance, but they are also unable to move through the diode's junction capacitance. Thus, the net charge transferred to the hold capacitor must be zero. In other words, while electrons can be stored temporarily on the moving "plates" formed by the depleted region in the diode's junction, resulting in short-lived currents in the circuit, no net charge can be moved through the junction capacitance to the hold capacitor. As a result, the impulse response, which is proportional to the *net* charge moved through the diode to the hold capacitor, must be zero.

A sampling circuit with $g(t) = 0$ and capacitance $C(t)$ shown in Fig. 6, illustrates this idea nicely. The circuit's equivalent circuit, normalized impulse response, and kickout pulse are shown in Fig. 7. Charge conservation requires that the total charge on the bottom plate of the diode's junction capacitance and the top plate of hold capacitor, which are enclosed by the dashed line in the figure, be conserved throughout the sampling cycle. There is nothing to prevent charge on these two capacitor plates from "sloshing" back and forth between the two capacitor plates, generating the kickout pulse shown in Fig. 7. However, charge conservation does not allow the net charge on the two capacitor plates to change during the sampling cycle. Thus, no net charge is transferred onto the hold capacitor during sampling operation, and the impulse response is identically equal to zero.

VIII. Conclusion

We have developed an analytic small-signal model of a balanced two-diode sampling circuit that includes time-varying diode junction capacitance and conductance. We used this model to explore the effects of the diode's junction capacitance and conductance on the kickout pulses and impulse response of the sampling circuit, which the nose-to-nose technique assumes are identical.

We found that when the diode conductance is symmetric and the junction capacitance is either zero or constant, the normalized kickout pulses and impulse response are identical. However, when the diode conductance is asymmetric, the time reversal inherent in (15) leads to differences in the kickout pulses and impulse response that cannot be corrected for by the nose-to-nose calibration. These conclusions are consistent with those of [1]–[3].

We found that it is not possible to express the kickout pulse and impulse response as the simple convolution of an aperture circuit function and a time-invariant response function of the external circuitry. This is because the sampling diodes interact directly with other circuit elements that are physically close enough to be affected by the diodes' time-varying conductance and capacitance during the sampling aperture [2], [3]. We conclude that linear circuit elements in close proximity to the diode may need to be included in nonlinear circuit models of the sam-

pling circuit, if the differences in the kickout pulses and impulse response are to be precisely modeled.

We also saw that changes in the diode's junction capacitance play a direct role in the generation of kickout pulses. This is because the kickout is proportional to the *instantaneous* small-signal current flowing through the diode, which depends on changes in the diode's junction capacitance. On the other hand, the impulse response is related to the *net* charge transferred to the hold capacitor during a complete sampling cycle. Since electrons are unable to move through the diode's junction capacitance, all of this charge must move through the diode's conductance. Therefore, the junction capacitance has little effect on the impulse response. These two contrasting physical phenomena can give rise to significant differences in the sampler's kickout pulses and impulse response. As a consequence, we conclude that accurate models of the sampling circuitry must include the diode's nonlinear junction capacitance.

APPENDIX I
CONSTANT CAPACITANCE

Here, we summarize the analytic solutions for the kickout pulses and impulse response when the junction capacitance $C = C_0$ is constant. The conductance function $g(t)$ is equal to zero for $t < -t_g/2$, equal to g_0 for $-t_g/2 < t < 0$, equal to g_1 for $0 < t < t_g/2$, and equal zero for $t > t_g/2$. These solutions correspond to the kickout pulses and impulse responses plotted in Figs. 3 and 4. The solution for a normalized kickout pulse v'_k is shown in (16) at the bottom of this page, and the solution for the normalized impulse response v'_s is shown in (17) at the bottom of this page, where $g'_0 \equiv (R'+R_s)g_0$, $g'_1 \equiv (R'+R_s)g_1$, and $C'_0 \equiv (R'+R_s)C_0$.

APPENDIX II
TIME-VARYING CAPACITANCE

We also obtained analytic solutions for the kickout pulses and impulse response when the diode conductance and capacitance take the form illustrated in Fig. 6. Here, $g(t)$ equals zero for $t < -t_g/2$, g_0 for $-t_g/2 < t < t_g/2$, and zero again for $t > t_g/2$, while $C(t)$ equals C_0 for $t < -t_-$, increases linearly from C_0 to $C_0 + \Delta C$ over the region $-t_- < t - t_g/2$, equals $C_0 + \Delta C$ over the region $-t_g/2 < t < t_g/2$, decreases linearly from $C_0 + \Delta C$ to C_0 over the region $t_g/2 < t < t_+$, and equals C_0 for $t > t_+$. This case corresponds to the kickout pulse and impulse response plotted in Fig. 5.

A. Normalized Kickout Pulses

For $t \le -t_-$, we have $v'_k(t) = 0$. In the region $-t_- \le t \le -t_g/2$, the solution for v'_k is

$$v'_k(t) = \frac{1}{\gamma_-}\left[1 - \left(\frac{C(t)}{C_0}\right)^{-\gamma_-}\right] \tag{18}$$

where

$$\gamma_- \equiv \frac{1 + (R' + R_s)\Delta C/\left(t_- - (t_g/2)\right)}{(R' + R_s)\Delta C/\left(t_- - (t_g/2)\right)}. \tag{19}$$

In the region $-t_g/2 \le t \le t_g/2$, v'_k is

$$v'_k(t) = \frac{g'_0}{1+g'_0}\left[1 - \exp\left(-\frac{1+g'_0}{C'_0 + \Delta C'}\left(t + \frac{t_g}{2}\right)\right)\right] + v'_k\left(-\frac{t_g}{2}\right)\exp\left(-\frac{1+g'_0}{C'_0 + \Delta C'}\left(t + \frac{t_g}{2}\right)\right) \tag{20}$$

$$v'_k(t) = \begin{cases} 0, & t \le -\dfrac{t_g}{2} \\ \dfrac{g'_0}{1+g'_0}\left[1 - \exp\left(-\dfrac{1+g'_0}{C'_0}\left(t + \dfrac{t_g}{2}\right)\right)\right], & -\dfrac{t_g}{2} \le t \le 0 \\ \dfrac{g'_1}{1+g'_1}\left[1 - \exp\left(-\dfrac{1+g'_1}{C'_0}t\right)\right] + v'_k(0)\exp\left(-\dfrac{1+g'_1}{C'_0}t\right), & 0 \le t \le \frac{t_g}{2} \\ v'_k\left(\dfrac{t_g}{2}\right)\exp\left(-\dfrac{t - (t_g/2)}{C'_0}\right), & \dfrac{t_g}{2} \le t \end{cases} \tag{16}$$

$$v'_s(\tau) = \begin{cases} 0, & \tau \le -\dfrac{t_g}{2} \\ \dfrac{g'_1}{1+g'_1}\left[1 - \exp\left(-\dfrac{1+g'_1}{C'_0}\left(\tau + \dfrac{t_g}{2}\right)\right)\right], & -\dfrac{t_g}{2} \le \tau \le 0 \\ \dfrac{g'_0}{1+g'_0}\left[1 - \exp\left(-\dfrac{1+g'_0}{C'_0}\tau\right)\right] + v'_s(0)\exp\left(-\dfrac{1+g'_0}{C'_0}\tau\right), & 0 \le \tau \le \dfrac{t_g}{2} \\ v'_s\left(\dfrac{t_g}{2}\right)\exp\left(-\dfrac{\tau - (t_g/2)}{C'_0}\right), & \dfrac{t_g}{2} \le \tau \end{cases} \tag{17}$$

where $\Delta C' \equiv (R' + R_\mathrm{s})\Delta C$. In the region $t_\mathrm{g}/2 \le t \le t_+$, v'_k is

$$v'_\mathrm{k}(t) = v'_\mathrm{k}\left(\frac{t_\mathrm{g}}{2}\right)\left(\frac{C(t)}{C_0+\Delta C}\right)^{\gamma_+} - \frac{1}{\gamma_+}\left[1-\left(\frac{C(t)}{C_0+\Delta C}\right)^{\gamma_+}\right] \tag{21}$$

where

$$\gamma_+ \equiv \frac{1-(R'+R_\mathrm{s})\Delta C/\left(t_+ - (t_\mathrm{g}/2)\right)}{(R'+R_\mathrm{s})\Delta C/\left(t_+ - (t_\mathrm{g}/2)\right)}. \tag{22}$$

Observe that γ_+ is not equal to γ_-. This is because γ_- describes the charging of the capacitor as its capacitance increases, while γ_+ describes the discharging of the capacitance while its capacitance is decreasing. In the region $t \ge t_+$

$$v'_\mathrm{k}(t) = v'_\mathrm{k}(t_+)\exp\left(-\frac{t-t_+}{C'_0}\right). \tag{23}$$

B. Normalized Impulse Response

In the region $\tau \le -t_\mathrm{g}/2$, $v'_\mathrm{s}(\tau) = 0$. In this time region, the impulse arrives after the diode conductance has reset itself to zero, and the impulse response is zero. This region also includes the times $\tau \le -t_+$ and, thus, t_+ does not play a role in determining the sampler's impulse response. In the region $-t_\mathrm{g}/2 \le \tau \le t_\mathrm{g}/2$, v'_s is

$$v'_\mathrm{s}(\tau) = \frac{g'_0}{1+g'_0}\left[1-\exp\left(-\frac{1+g'_0}{C'_0+\Delta C'}\left(\tau+\frac{t_\mathrm{g}}{2}\right)\right)\right]. \tag{24}$$

In the region $t_\mathrm{g}/2 \le \tau \le t_-$, v'_s is

$$v'_\mathrm{s}(\tau) = v'_\mathrm{s}\left(\frac{t_\mathrm{g}}{2}\right)\left(\frac{C(-\tau)}{C_0+\Delta C}\right)^{\gamma_- - 1}. \tag{25}$$

In the region $\tau \ge t_-$

$$v'_\mathrm{s}(\tau) = v'_\mathrm{s}(t_-)\exp\left(-\frac{\tau-t_-}{C'_0}\right). \tag{26}$$

ACKNOWLEDGMENT

The authors wish to thank Dr. J. Verspecht, Agilent Technologies, Brussels, Belgium, for his careful reading of this paper's manuscript and the numerical analysis he performed to verify the authors' analytic results.

REFERENCES

[1] J. Verspecht and K. Rush, "Individual characterization of broadband sampling oscilloscopes with a nose-to-nose calibration procedure," *IEEE Trans. Instrum. Meas.*, vol. 43, pp. 347–354, Apr. 1994.

[2] J. Verspecht, "Broadband sampling oscilloscope characterization with the 'nose-to-nose' calibration procedure: A theoretical and practical analysis," *IEEE Trans. Instrum. Meas.*, vol. 44, pp. 991–997, Dec. 1995.

[3] ——, "Calibration of a measurement system for high frequency nonlinear devices," Ph.D. dissertation, Dept. Elect., Free Univ. Brussels, Brussels, Belgium, 1995.

[4] D. F. Williams, K. A. Remley, and D. C. DeGroot, "Nose-to-nose response of a 20-GHz sampling circuit," in *54th ARFTG Conf. Dig.*, Dec 1999, pp. 64–70.

[5] K. A. Remley, D. F. Williams, and D. C. DeGroot, "Realistic sampling circuit model for a nose-to-nose simulation," in *2000 Int. Microwave Symp. Dig.*, June 2000, pp. 1473–1476.

[6] K. A. Remley, D. F. Williams, D. C. DeGroot, and J. Verspecht, "Effect of nonlinear diode junction capacitance on the nose-to-nose claibration," *IEEE Microwave Wireless Comp. Lett.*, May 2001, to be published.

[7] K. Rush, S. Draving, and J. Kerley, "Characterizing high-speed oscilloscopes," *IEEE Spectr.*, pp. 38–39, Sept. 1990.

[8] M. Braum, "Differential equations and their applications," in *Applied Mathematical Sciences*. Berlin, Germany: Springer-Verlag, 1975, vol. 15.

Dylan F. Williams (S'82–M'86–SM'90) received the Ph.D. degree in electrical engineering from the University of California at Berkeley, in 1986.

In 1989, he joined the Electromagnetic Fields Division, National Institute of Standards and Technology, Boulder, CO, where he currently develops metrology for the characterization of monolithic microwave integrated circuits and electronic interconnects. He has authored or co-authored over 60 technical papers.

Dr. Williams was the recipient of the Department of Commerce Bronze and Silver Medals, the Electrical Engineering Laboratory's Outstanding Paper Award, two Automatic RF Techniques Group (ARFTG) Best Paper Awards, the ARFTG Automated Measurements Technology Award, and the IEEE Morris E. Leeds Award.

Kate A. Remley (S'91–M'99) was born in Ann Arbor, MI, in December 1959. She received the B.S. degree (*magna cum laude*), M.S. degree, and Ph.D. degree in electrical and computer engineering from Oregon State University, Corvallis, in 1993, 1995, and 1999, respectively.

From 1983 to 1992, she was a Broadcast Engineer. From 1989 to 1991, she was a Chief Engineer of an AM/FM broadcast station. In 1999, she joined the Radio-Frequency Technology Division, National Institute of Standards and Technology, Boulder, CO, where she is currently a Research Engineer. Her research activities focus on development of metrology for nonlinear circuits used in wireless communication systems.